Storm-source geometry biases mantle transition-zone water estimates from a century-scale geomagnetic archive

Seokhoon Oh

Department of Energy and Resources Engineering, Kangwon National University, Chuncheon 24341, Republic of Korea

Corresponding author. Email: gimul@kangwon.ac.kr

ORCID: https://orcid.org/0000-0002-3670-3336

Peer-review status. This is a non-peer-reviewed preprint submitted to EarthArXiv. It is intended for submission to a peer-reviewed journal.

Companion papers. The physical mechanism is established in a companion manuscript under review at *Science*; the processing chain is described in a methods companion under review at *Earth, Planets and Space* (EPSP-D-26-00179).

Data and code. All input data are public (INTERMAGNET; WDC Kyoto; SILSO; CHAOS-7). Code, locked archives, and the gate ledger: https://doi.org/10.5281/zenodo.21184326 (v1.1 adds the audit layer).

License. CC BY 4.0.

Abstract

Electromagnetic estimates of water in the mantle transition zone depend on the assumed geometry of storm-time source fields. We audit the effect of that assumption using paired processing chains that differ only by inclusion of a degree-3 zonal source term, together with pre-specified admission gates. The experiment is applied to three separately processed, partially overlapping observatory records spanning 6, 15, and 80 years and to random subnetworks drawn from a century-scale station pool. At 12 stations, 58 to 62% of random draws fail the admission gate; failed chains produce apparent transition-zone shifts of 2.5 to 3.4 decades and are not physically interpretable. Among admitted sparse draws, shifts range from −0.30 to +0.65 decades and have draw-dependent sign. By contrast, the tested curated networks at 12, 43, and 130 stations give mutually consistent legacy-minus-source-aware shifts near −0.13 decades, indicating that the degree-1-only chain underestimates conductivity. Co-estimating the degree-3 term in the 1940 to 2020 chain improves normalized misfit from 1.41 to 1.07 and yields a transition-zone conductivity of 0.386 S/m. Laboratory conductivity–water calibrations map the curated-network shift to a dry-bias factor of 1.25 to 1.55; admitted sparse networks can produce larger errors in either direction. The published conductivity range overlaps the validated sparse-network envelope, although attribution to individual studies requires controlled paired reanalysis. These results identify two source-geometry risks: a systematic, correctable dry bias in the tested curated chains and sign-unstable errors in unbalanced sparse networks.

Keywords: geomagnetic depth sounding; mantle transition zone; electrical conductivity; source field geometry; historical geomagnetic archives; mantle water

1. Introduction

Electrical conductivity is the principal geophysical window on water in the mantle transition zone. Hydrogen dissolved in wadsleyite and ringwoodite raises conductivity by orders of magnitude (Karato, 1990; Huang et al., 2005; Yoshino et al., 2008). Conductivity profiles built from geomagnetic observatory records are therefore read, through laboratory calibrations, as water meters for the deep mantle. Published estimates disagree, and the disagreement has been attributed to data coverage, regularization, and the laboratory calibration debate (Karato and Dai, 2009; Yoshino and Katsura, 2012, 2013).

A companion paper (Oh, 2026a) isolated a further term in this error budget, on the source side of the measurement. The storm-time source field carries a small degree-3 zonal component (P_3^0). Its storm-band coherent part is phase-locked nearly opposite to the dominant ring-current field. Through a phase-selective transfer, omitting this component biases recovered transition-zone conductivity, and the size of the bias is governed by network sparsity and geometry. That paper isolates the mechanism. What the mechanism did to the accumulated archive is a separate question, and it is the subject of the present work.

The unresolved question is therefore not whether source geometry can affect an induction response, which is classical, but whether it has measurably affected the historical conductivity archive from which mantle water estimates have been inferred, and by how much. This paper answers that question: what did the bias do to the historical observatory record, chain by chain, era by era, and what can be repaired. The century archive is heterogeneous. Station networks grew from a handful of observatories to more than a hundred. Processing conventions changed. Validation culture, in the modern sense of pre-specified acceptance gates and negative controls, did not exist for most of the record. We therefore proceed in four steps. (i) We build an audit machinery: a validation taxonomy with pre-specified admission gates that separates chains whose output is interpretable from chains that have collapsed. (ii) We measure the error of passing chains across network regimes, using three separately processed observatory records and random-subnetwork envelopes. (iii) We correct the century chain by co-estimating the degree-3 term with era gates, and we translate the correction into absolute water content using laboratory constants digitized from the original publications.

(iv) We compare the structure of the historical literature's transition-zone conductivity spread against our envelopes.

The division of labor with the companion paper is explicit. The companion establishes the mechanism, the phase carrier, and the injection closure (Oh, 2026a). The audit protocol, the three-record machinery, the era-gated correction, the absolute water panel, and the literature comparison are original to this paper. The two papers share no figures, and the one sign convention difference between them is stated in Section 2.4.

2. Data and processing chains

2.1 Three records

Three separately processed hourly records support the audit; they overlap in time but differ in station set, era, and internal-field treatment. First, a six-year, twelve-observatory record (2014 to 2019) retrieved from INTERMAGNET, the discovery record of the companion paper. Second, a fifteen-year, 57-observatory archive (2010 to 2024), of which 43 stations pass a continuity filter. Third, a century-scale archive of 130 observatories, era-gated to 1940 to 2020, assembled from World Data Centre holdings. The three records differ in data source, station set, era, and internal-field treatment. Their processing shares one frozen pipeline: core-field removal, quality control, rotation to centered-dipole coordinates, epoch-wise spherical-harmonic source separation by weighted least squares, robust transfer-function estimation designed for gapped records, and regularized 1-D inversion. The chain is described in the methods companion (Oh, 2026b) and in the supplementary materials of Oh (2026a). It enters the audit frozen and unmodified, so the paired comparisons below cannot be artifacts of method tuning.

2.2 The paired experiment

Every audit below rests on one paired comparison. Two configurations of the identical chain differ only in the source basis of the epoch-wise separation. The reference configuration separates the degree-1 terms alone (P_1^0 with the two m=1 terms), the standard assumption of the C-response lineage. The corrected configuration adds the degree-3 zonal term (3,0), two coefficients per epoch.

The physical basis for that specific term, needed here only in outline, is as follows. The storm-time ring current is an extended equatorial current, not a point dipole. Its multipole expansion carries a degree-3 zonal term. The ratio of this term to degree-1 is negative and of order $(a/b)^2$, where b is the current distance (Daglis et al., 1999). Oh (2026a) measures the term directly. This is a magnetospheric, storm-band, zonal harmonic, distinct from the non-axisymmetric ionospheric-tidal degree-3 mode (3,2) treated in source-aware satellite inversions (Min and Grayver, 2023). Because it is nearly anti-phase to the dominant degree-1 field, a network that cannot separate it does not lose it; it folds the unmodelled degree-3 response into the apparent degree-1 channel, which the inversion then reads as a change in mantle conductivity. The present audit does not rederive that mechanism. It only adds or removes the (3,0) basis vector and measures what the difference does to the recovered profile.

The (1,0) coefficient pair is the induction channel used downstream in both configurations. The response we invert is the degree-1 ratio $Q \equiv \iota_1^0/\varepsilon_1^0$ of the internal (induced) to external (inducing) coefficient, the standard C-response expressed as a dimensionless ratio. The paired difference therefore isolates the source model: Earth model, frequency bins, uncertainties, and regularization are shared, so the paired design minimizes sensitivity to shared Earth-model error and responds mainly to the change of source basis.

2.3 Admission gates

We classify each chain before interpreting it. A chain is admitted when its corrected configuration satisfies two pre-specified conditions, fixed before the envelope runs and archived in the deposited gate ledger: the anchor deviation (agreement of the recovered response with its own data-side reconstruction) is at most 25%, and the normalized misfit lies in [0.3, 3]. The normalized misfit is χ^2 per datum; because the number of data far exceeds the number of model parameters, it approximates the reduced chi-square, and its target value is one. Chains failing either condition are labeled failed (non-interpretable) and their outputs are reported but not interpreted. The gate was fixed before the envelope runs. The three-phase result does not depend on the exact thresholds. Across a grid of anchor cut at 20, 25, and 30% and reduced-misfit band [0.5, 2], [0.3, 3], and [0.2, 5], the sparse collapse fraction stays between 50 and 75% (Table S1). The admitted-shift medians of that small ensemble are superseded by the larger ensembles of Table S2. Synthetic controls for the gate and for the paired machinery are described in Section 3.3.

The gate is complementary to response-level realizability tests of the D+ class (Parker, 1980), which reject individual response estimates inconsistent with any 1-D conductor and are standard practice in the field (Olsen, 1999). Those tests operate downstream of the source separation. They cannot detect a collapsed separation that produces a smooth, realizable, and wrong response, which is exactly the failure class the paired-configuration anchor and misfit conditions target.

2.4 Sign convention

Throughout this paper, ΔTZ denotes the transition-zone (450 to 670 km) shift in $\log_{10}$ conductivity, $\Delta\log_{10}\sigma$_TZ, in the sense WITHOUT minus WITH: $\Delta TZ \equiv \log_{10}\sigma(P_1^0\text{-only}) - \log_{10}\sigma(P_1^0{+}P_3^0)$. A negative ΔTZ means the legacy configuration underestimates conductivity, hence underestimates water. Shifts are quoted in decades, where one decade is one order of magnitude in conductivity. The companion paper quotes the same quantity in the opposite sense (corrected minus legacy). Its +0.135 and our −0.135 are the same measurement.

Every quoted uncertainty on a paired shift is one bootstrap standard deviation: the response is resampled within its estimation errors, carried through the inversion, and the standard deviation of the resulting transition-zone shifts is reported. The "4σ" attached to the century value means the estimate lies 4.0 bootstrap standard deviations from zero. These uncertainties reflect response-estimation and resampling noise; they do not add an absolute Earth-model or calibration term, which the paired design holds fixed.

3. The audit machinery

3.1 Random-subnetwork envelopes

From the century pool we draw random subnetworks at 12, 24, and 48 stations (eight draws each at 12 and 24, four at 48) and run the full paired experiment on each draw. The draws are not curated. They emulate the geometric freedom of historical station selection without expert balance. Each draw is classified by the admission gate before its ΔTZ is read. The main-text envelope uses eight draws per sparse size; two independent enlargements to thirty and sixty draws per size confirm the collapse fractions and show that the admitted shift is sign-unstable, correcting the small-sample impression of a uniformly positive sparse shift (Table S2).

3.2 Era gates

The century chain is era-gated to 1940 to 2020 after diagnostic scans of chain-index correlation and baseline behavior; the same diagnostics motivate the era gating of the fifteen-year archive reported in the companion.

Era gates are part of the audited chain, not a post hoc filter: the corrected century configuration passes the admission gate with the era gate in place (normalized misfit 1.41 without the degree-3 term, 1.07 with it). Earlier century-scale observatory inversions used a fixed time window without such gating (Tarits and Mandéa, 2010).

3.3 Synthetic controls

Two synthetic controls calibrate the machinery. A negative control runs the full paired experiment on a synthetic world with no (3,0) source term. The paired shift is $|\Delta TZ| \leq 0.002$ for both test geometries. The machinery does not manufacture the effect it measures. A positive control injects a degree-3 source and asks whether the paired experiment recovers it. An early variant with a synthetic in-phase ε_3 proved the capacity of the mechanism (paired shifts of 0.45 to 0.85 with misfit degradation when the term is omitted) but produced the opposite sign, which identified the injected phase as the controlling property. The definitive positive control therefore injects the measured ε_3^0 series itself. It reproduces the sign of the real-data effect and 74% of its magnitude (paired shift +0.176 against +0.239, corrected minus legacy), and a latitude-limited variant confirms the dependence on latitude span. The phase dependence of the sign is the companion paper's mechanism; here it serves as a closed-loop check that the audit machinery measures a source property, not an analysis artifact.

3.4 Sq hygiene

The non-zonal terms of the source-aware separation absorb part of the daily solar-quiet variation, which contaminates long-period observatory records (Malin and Winch, 1996). A per-station sun-synchronous Sq removal, adopted as standard preprocessing for the century chain, changes the broadband (3,0) diurnal content but leaves the storm-band carrier and the symmetric ε_1^0 channel essentially unchanged. The audit results below are robust to this choice.

4. Results

4.1 A three-phase structure

The envelopes reveal three regimes (Fig. 3).

Collapse phase. At twelve stations, 58 to 62% of random draws fail the admission gate, stable across three independent ensembles totalling 98 draws; at twenty-four stations the failure fraction is 30 to 50% (Table S2). Failures are not subtle. Anchor deviations reach 311% at 12 stations and 198,632% at 24 stations in the worst draws. Their apparent paired shifts reach $|\Delta TZ|$ of 2.5 to 3.4 decades. Every such case is caught by the gate. At these network sizes an uncurated chain often cannot support the separation at all, and its output does not carry a usable measurement. In earlier decades such a chain could have been reported as a result. We make no attribution to any individual historical study; Section 4.4 states what can and cannot be concluded.

Sparse admitted phase. Random draws that pass the gate do not share a sign. Across the discovery envelope and two independent enlargements (98 draws at each sparse size; Table S2), admitted twelve-station shifts span −0.30 to +0.65 decades with a median magnitude near 0.2, and the sign splits close to evenly (19 positive, 21 negative). In water terms (Section 4.3) an admitted sparse draw misreads water by a factor of up to about 2 to 4, in a direction set by the draw geometry, not by the mantle. The three uniformly positive admitted draws of the eight-draw discovery envelope were a small-sample fluctuation, identified by the enlarged ensembles.

Dense convergent phase. The full 130-station century chain gives a paired shift of -0.135 ± 0.034 decades, alongside the fifteen-year 43-station archive at -0.112 ± 0.067. Of the four 48-station discovery draws, two pass the admission gate, both near zero (+0.02 and −0.01); the sample is too small to locate a regime crossover robustly.

That admitted sparse draws scatter in both directions while curated networks share one sign is the phase-selective leakage mechanism at work (Oh, 2026a): the sign and size of the aliased term depend on the draw geometry, and only balanced networks pin it down. The audit contribution is the regime map.

4.2 Three-record concordance: balance, not count

The three curated records agree (Fig. 5). In the WITHOUT−WITH convention, the six-year twelve-station record gives −0.239 ± 0.177, the fifteen-year 43-station archive −0.112 ± 0.067, and the century 130-station chain −0.135 ± 0.034. Data sources, eras, station sets, and internal-field treatments differ across the three; the overlap near −0.13 decades is the common curated-network systematic. Against this, random draws of the same sizes scatter with unstable sign (Section 4.1). The controlling variable is therefore geometric balance, not station count. A curated twelve-station network behaves like the dense limit in sign; a random twelve-station network usually does not, when it works at all.

One bookkeeping correction is recorded here because earlier internal reports propagated it. The six-year record's widely quoted 0.47-decade figure is an envelope-distance metric (distance of the recovered profile from a three-profile benchmark), not a paired layer shift. The correct paired shift of the six-year record is −0.239 ± 0.177 as above. Figure captions in this paper use the paired convention throughout.

4.3 Era-gated correction and the absolute water panel

Correcting the century chain costs two coefficients per epoch. With the (3,0) term co-estimated and era gates in place, the century chain passes the admission gate with improved misfit (1.41 to 1.07) and yields a corrected transition-zone conductivity of 0.386 S/m.

To translate paired shifts into water content we digitized calibration constants from the original laboratory publications (Dai and Karato, 2009a, Table 2; Yoshino and Katsura, 2012; Yoshino and Katsura, 2013, Table 1; Dai and Karato, 2009b, for garnet). As a check we reproduced each source's own worked example (0.148 S/m against the published value of about 0.1 S/m at 1700 to 1800 K and 0.1 wt%). Both calibration branches use a two-mechanism sum, a polaron branch and a proton branch, so the water-content bias factor is computed by inverting the full law rather than a power-law shortcut. We report the apparent water factor in the sense legacy over corrected, so that a curated network reading too dry appears below one; the equivalent "too low by a factor of" statements in the text are its reciprocal. The result is a bracket per network regime, with the two laboratory branches as the bracket ends (Fig. 4):

Dense modern networks ($\Delta TZ = -0.135$): inferred water is too low by a factor of 1.25 (Yoshino branch) to 1.55 (Karato branch). Under the water-exponent uncertainty of the Karato branch ($r = 0.72 \pm 0.08$) the dry end widens to 1.48 to 1.64.

Random sparse admitted networks (draw-dependent sign): at a representative admitted magnitude of 0.4 decades water is misread by 1.9 (Yoshino) to 3.6 (Karato) on wet-side draws and by the near-reciprocal division of 2.0 to 3.7 on dry-side draws. At the ensemble median magnitude of 0.2 decades the factors are 1.4 to 1.9 either way. The largest single admitted draw (+0.65 decades) reaches about 4.3. The calibration is nearly symmetric in the logarithm, so the two directions carry the same brackets.

The factors are invariant to within ±2% across mantle temperature 1750 to 1900 K and mixing exponent β of 0.6 or 1.0, so the disputed absolute calibrations enter only as the bracket ends, not through temperature or mixing assumptions. A split of the transition zone into wadsleyite and ringwoodite layers is not resolvable in this chain (inter-layer correlation +0.86), so the panel treats the transition zone as one layer.

The regime asymmetry is the central archive-level fact. Curated chains, at any size and in all three records, read the transition zone too dry by a systematic and correctable amount. Random unbalanced chains are not systematically biased in either direction; they are unreliable, with draw-dependent sign and magnitudes up to several times the curated systematic. An archive user therefore faces two failure modes: a correctable bias when the network is well balanced, and an unpredictable error when it is not. For reference, and not as a claim, we give the corresponding absolute water contents. At 1800 K and $\beta = 0.6$ the corrected conductivity of 0.386 S/m gives 0.63 wt% on the Karato branch and 1.28 wt% on the Yoshino branch. At $\beta = 1.0$ the Karato branch gives 0.31 wt%, of the same order as the 0.1 to 0.2 wt% inferred for the Pacific transition zone by Huang et al. (2005).

4.4 The historical literature spread

We compiled fifteen published transition-zone conductivity estimates from thirteen studies spanning 1969 to 2022 into a common band (Fig. 6). Two comparisons discipline the interpretation. First, the compilation's scatter is consistent in width with our validated sparse-network envelope, and inconsistent with the dense convergent phase. Second, one controlled anchor exists. Olsen (1998) treated the same dataset both ways, with a single-harmonic Z/H route and a source-aware Z:Y route, and the single-harmonic route underestimated transition-zone conductivity by 0.24 decades while its squared coherence dropped from 0.92 to 0.62. The size matches our six-year paired shift, and the direction is the one our machinery predicts. This gives one historical case where the mechanism was caught in place.

What may be concluded is deliberately bounded. The published spread has many established contributors, among them one-dimensional versus three-dimensional structure, regularization, the ocean induction effect, the laboratory calibration debate, data selection, and the satellite versus observatory divide. Source geometry is an additional contributor, not a replacement for these. Our statement is the narrow one that the spread is quantitatively compatible with, and partly explainable by, a source-geometry contribution of the size our envelopes produce, and that this contributor has not previously been isolated. What may not be concluded is any attribution of an individual published profile to the collapse or sparse phase: classic networks were expert-curated rather than random, and our random envelopes bound the unbalanced regime, not the curated one. The three-record concordance (Section 4.2) shows what curation buys. Converting the compatibility into a decomposition requires controlled re-analyses of the kind the single Olsen (1998) anchor exemplifies, not the comparison of Fig. 6.

4.5 Generality of the audit checks

Three further measurements show that the same checks apply beyond the (3,0) term. First, a consensus-bias experiment with a local-time-fixed $m = \pm 1$ source shows single-station Z:H transfer functions biased by up to 52.7%, and no reweighting scheme can repair it; only spatial separation or explicit modeling can, which is the reason to co-estimate the source rather than correct the response afterwards. Second, per-storm geometry statistics on the real records give asymmetric-to-symmetric source ratios of 0.30 to 0.63, storm by storm, so a single frozen geometry cannot represent the storm population. Third, the degree allowance of a network is measurable in advance. At twelve stations the degree-2 zonal channel is not identifiable even when east-component rows are added to the separation (condition number 207), while the same east rows improve the conditioning of the production basis threefold. The admission diagnosis of Section 3 generalizes into a design rule for any future archive chain: measure how many source degrees the network can resolve, then include the degree that carries the bias.

5. Discussion

We address four questions about the reach of the audit.

Can collapse-phase results in the published record be identified? In principle yes, by re-running the admission gate on reconstructed chains, because the gate needs only the data and the chain's own configuration. In practice the required station lists and processing details are often not recoverable from the classic literature. We therefore provide the identification procedure and decline the attribution.

How far do the random envelopes reach? They bound the unbalanced regime. Expert curation demonstrably escapes it (Section 4.2), so the envelopes should be read as the risk profile of geometric freedom, historically largest in the eras with the fewest constraints on station choice.

What is the minimal requirement for the correction? Latitude span is the identifiability resource, not station count. The degree-allowance procedure of Section 4.5 gives the concrete test: an archive admits the (3,0) co-estimation when the separation's condition number at its actual station geometry remains within the audited range. Chains failing it should not attempt the correction; they should report exposure through the coherence diagnostic of the companion paper instead.

What upgrades the literature comparison from consistency to attribution? Controlled re-analyses. The single Olsen anchor shows the shape such evidence takes: one dataset, two source treatments, one direction of change. A program of such paired re-analyses on recoverable historical chains would convert Fig. 6 from a consistency statement into a measured decomposition of the literature spread.

Two limitations are inherited and stated. The chain is 1-D in Earth structure. This audit does not construct a new absolute water map. The two configurations share the same 1-D Earth, frequency bins, uncertainties, and regularization, so the paired difference reflects the source model rather than the Earth model. Three-dimensional structure, ocean induction, and lithospheric leakage are held fixed between the two configurations and are therefore largely common-mode. Residual interactions between the source-basis choice and lateral structure cannot, however, be excluded by the present 1-D analysis. Lateral heterogeneity otherwise enters only through the admission gate's misfit condition. The satellite-era global models that co-estimate source structure are outside the exposed population by construction (Oh, 2026a). Such joint source-and-conductivity inversion has been formalized recently (Min and Grayver, 2023; Püthe et al., 2015). The present audit is complementary: it targets the residual bias of already-published chains that cannot be re-inverted, rather than preventing the bias in a fresh inversion.

One point of scope is worth making explicit. The result reported here is the archive-level consequence of adding or removing the measured degree-3 source basis, and it stands on the paired experiment and controls of this paper. It does not require the reader to adopt the companion's full interpretation of the mechanism; the companion supplies the physical reading of why the (3,0) term takes the value it does, but the audit itself is a controlled test of what including that term does to eight decades of recovered profiles.

6. Conclusions

A pre-specified admission gate splits the historical archive's chains into a collapse phase, a sparse admitted phase, and a dense convergent phase. The collapse phase is common at historical network sizes and is fully detectable. Among admitted chains, geometric balance, not station count, decides the error. Three curated records spanning 6 to 80 years agree on a common systematic near 0.13 decades, while random unbalanced networks scatter with unstable sign several times larger. The correction costs two coefficients per epoch, passes the gate, improves misfit, and moves the century transition-zone conductivity to 0.386 S/m. Translated through laboratory calibrations digitized from the original sources, the omission biases curated chains dry by a factor of 1.25 to 1.55 at any network size, while random unbalanced chains misread water by draw-dependent factors of up to about 4 in either direction, with brackets stable to temperature and mixing assumptions. The historical spread of transition-zone water estimates is quantitatively compatible with this structure. The audit protocol, the correction, and the water panel are reusable as they stand, and every number regenerates from locked archives in the deposited code.

Figures

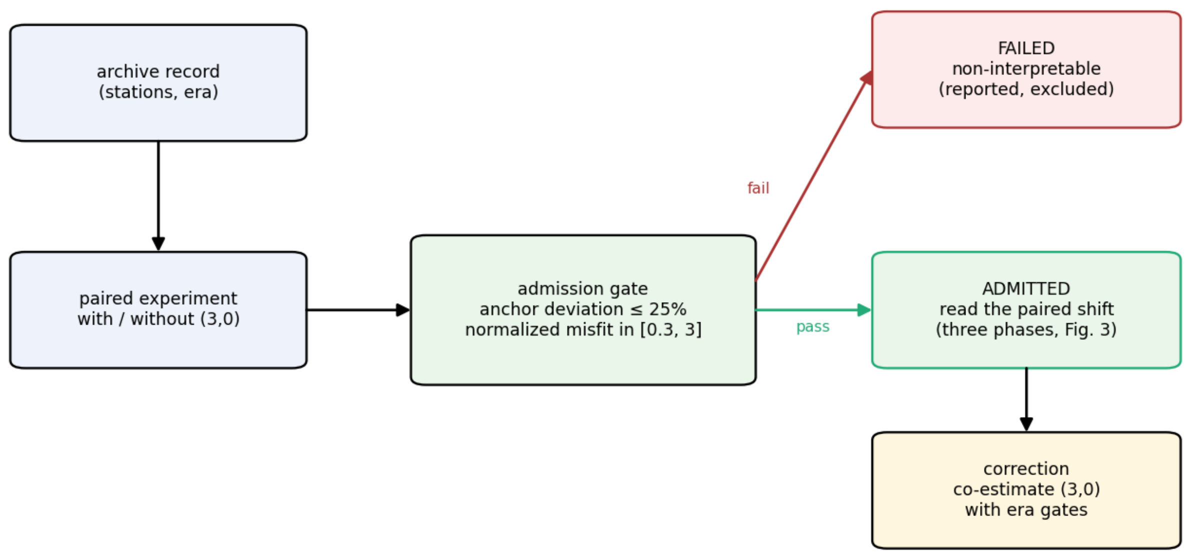

Fig. 1. Audit workflow. Each archive record is processed in paired source configurations. The corrected configuration is then evaluated against the pre-specified admission gate (anchor deviation $\leq 25\%$ and normalized misfit in [0.3, 3]). Failed chains are reported but excluded from physical interpretation. For admitted chains the paired transition-zone shift is read, and in the correction step the degree-3 term is co-estimated with era gating.

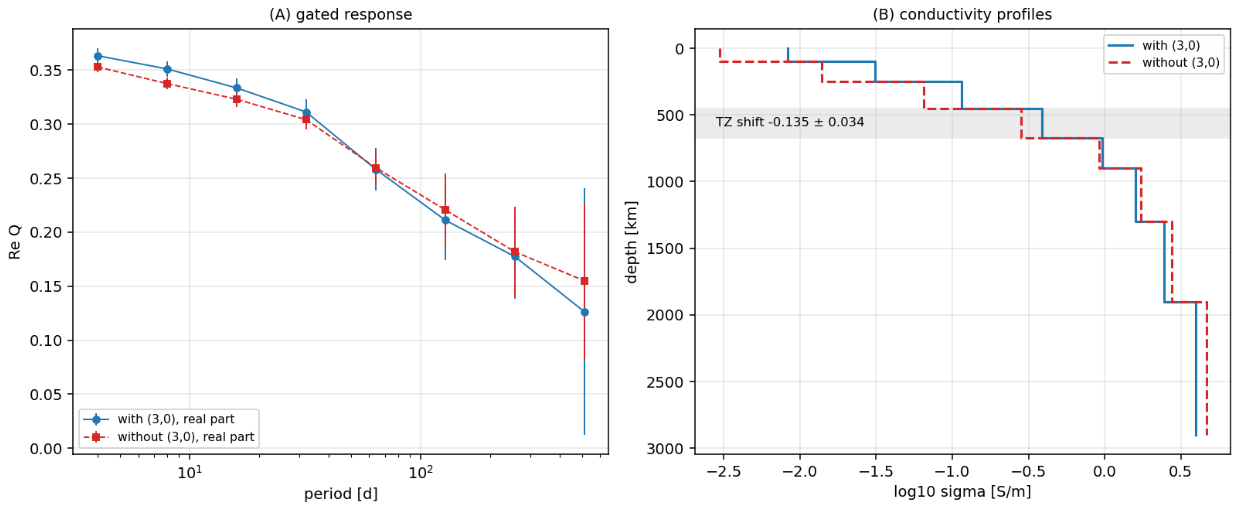

Fig. 2. Century chain, paired configurations. (A) Real part of the degree-1 response Q (the internal-to-external ratio $\iota_1^0/\varepsilon_1^0$) of the 130-station era-gated chain, with and without the (3,0) term. (B) Recovered conductivity profiles. The paired transition-zone shift is −0.135 ± 0.034 decades (WITHOUT−WITH); normalized misfit improves from 1.41 to 1.07.

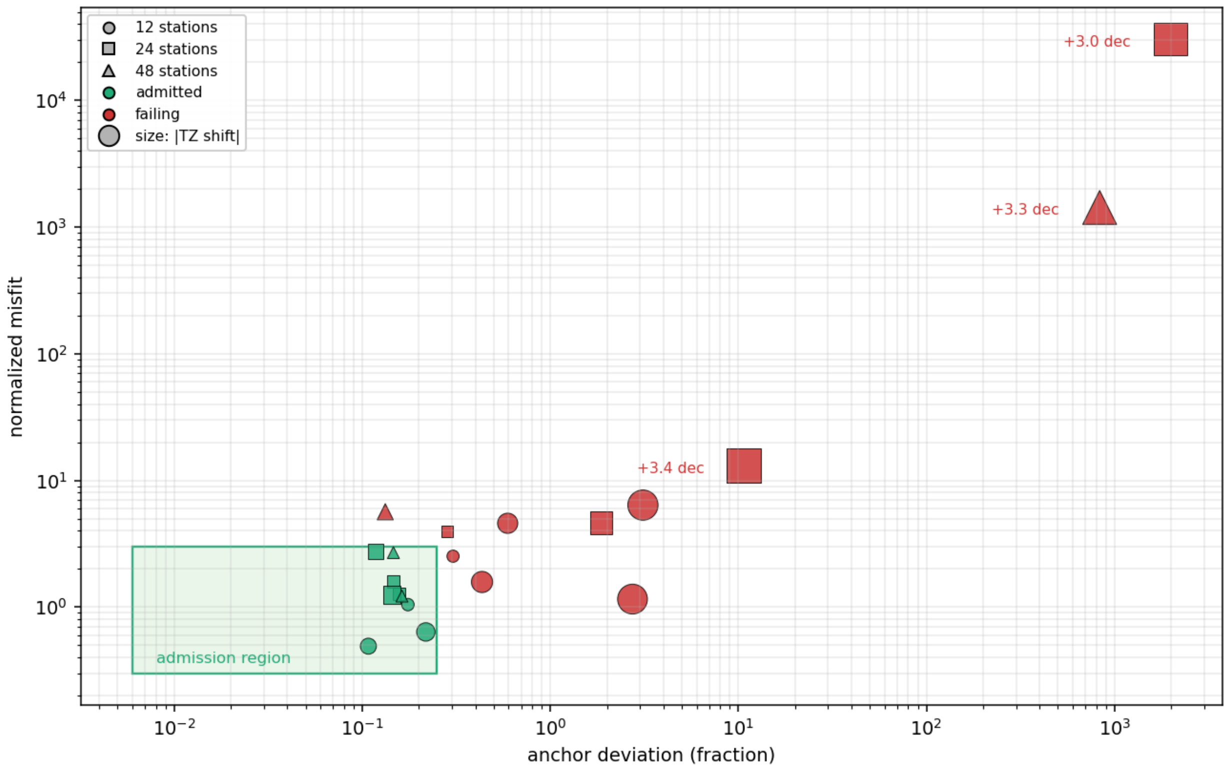

Fig. 3. The audit plane. Anchor deviation versus normalized misfit for the twenty random draws, with the admission region shaded. Green marks admitted draws and red marks failing draws. Marker shape gives the network size (12, 24, or 48 stations) and marker area scales with the apparent shift. Failing draws reach anchor deviations of 311% to 198,632%; the three largest apparent shifts (3.0 to 3.4 decades) are annotated. This panel shows the twenty-draw discovery ensemble; its three admitted twelve-station draws happen to be positive, but the independent thirty- and sixty-draw enlargements (Table S2) show sign-unstable admitted shifts with pooled medians near zero.

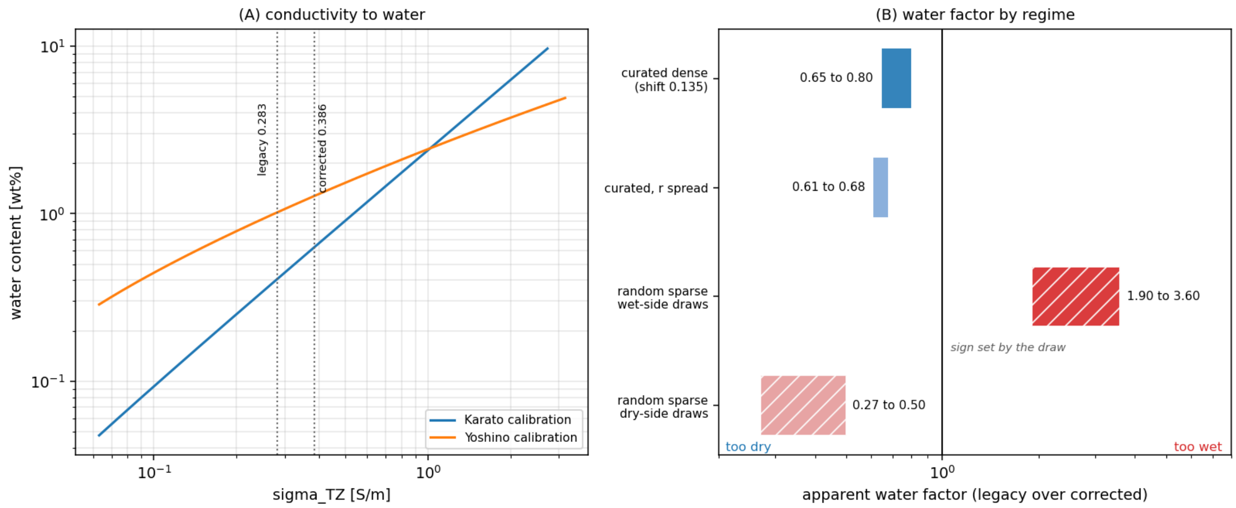

Fig. 4. Absolute water panel. (A) Conductivity to water inversion curves for both digitized calibrations at 1800 K and mixing exponent 0.6, with the legacy and corrected century conductivities marked. (B) Apparent water factor (legacy over corrected) per network regime. Curated dense networks read too dry (factors 0.65 to 0.80; the Karato-branch exponent sensitivity gives 0.61 to 0.68, so the combined curated envelope is 0.61 to 0.80). Random sparse admitted networks give a draw-dependent error (hatched): wet-side draws reach 1.9 to 3.6 and dry-side draws the near-reciprocal 0.27 to 0.50, with the sign set by the draw. Brackets span the two calibration branches; factors are invariant to ±2% over T = 1750 to 1900 K and β = 0.6 to 1.0.

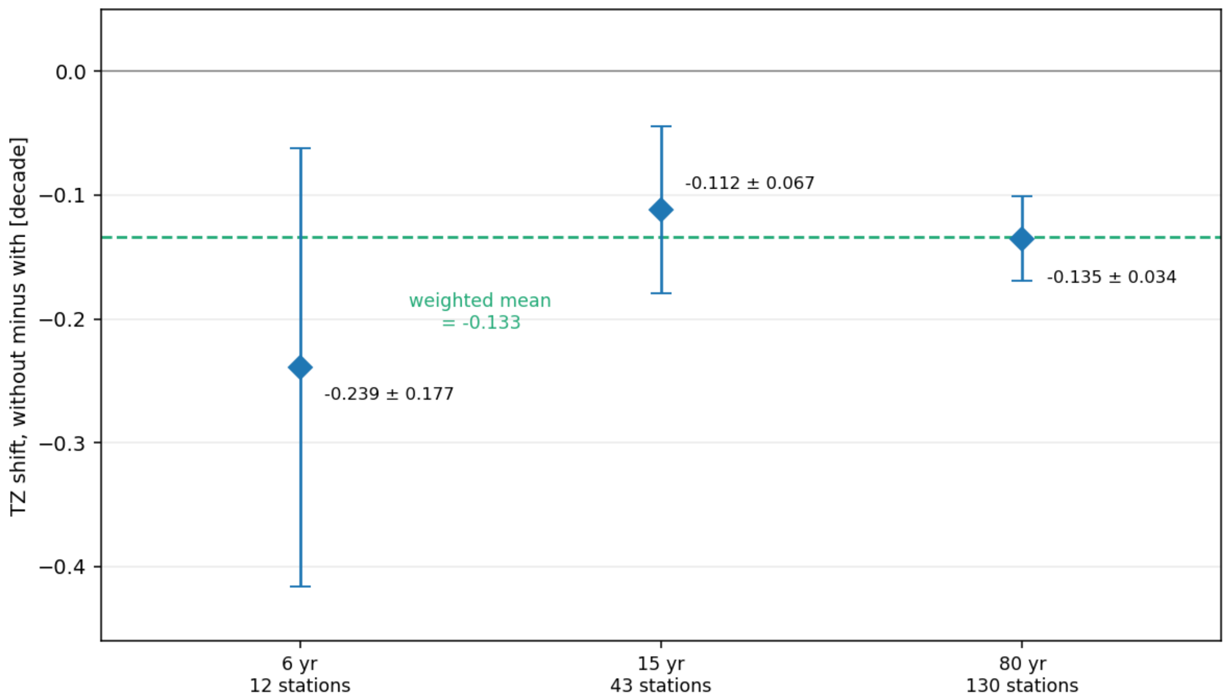

Fig. 5. Three-record concordance. Paired shifts of the three curated records: −0.239 ± 0.177 (six years, 12 stations), −0.112 ± 0.067 (fifteen years, 43 stations), −0.135 ± 0.034 (1940 to 2020, 130 stations). The inverse-variance-weighted mean is −0.133 decades (dashed), shown as a descriptive summary only; because the records overlap in time a formal combined uncertainty is not quoted. The concordance contrasts with the sign-unstable random envelope of Fig. 3.

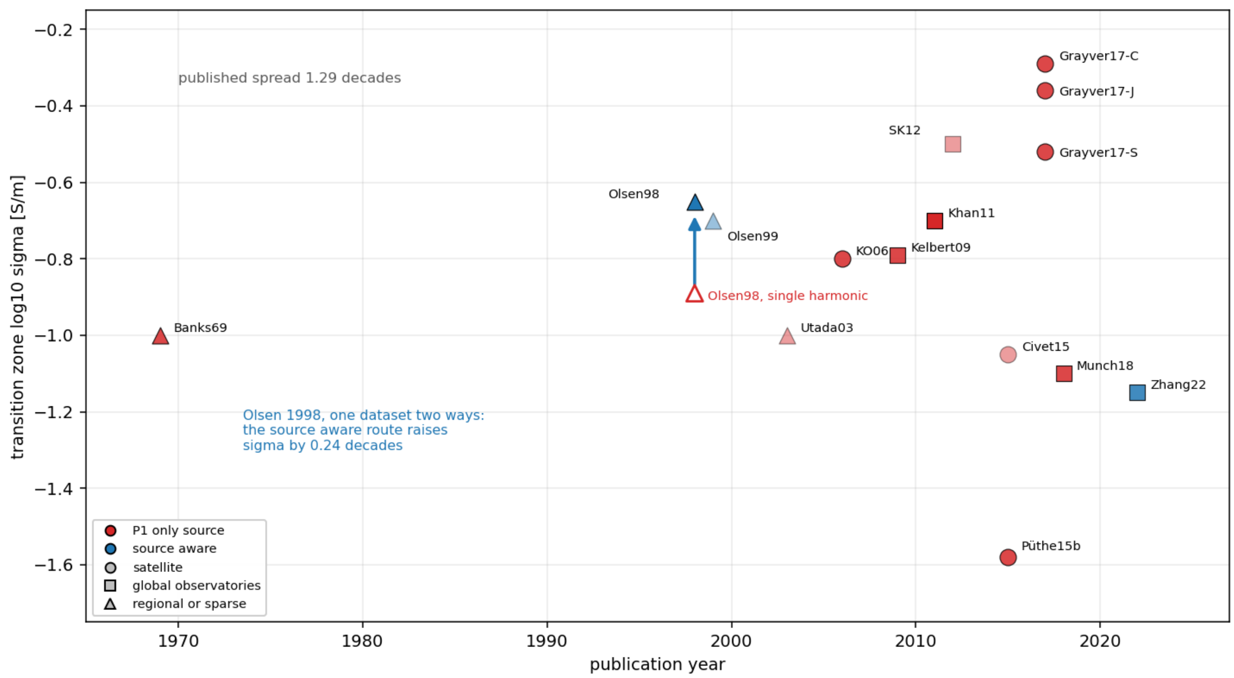

Fig. 6. Literature spread against the envelope. Fifteen published transition-zone conductivity estimates from thirteen studies (1969 to 2022). Color gives the source treatment (red: single-harmonic; blue: source-aware) and marker shape the network class. The published spread is 1.29 decades. The Olsen (1998) paired re-analysis is the single controlled anchor: the open triangle marks its single-harmonic value, and the arrow shows the source-aware treatment of the same data raising conductivity by 0.24 decades.

Supplementary Material

Table S1. Admission-gate threshold sensitivity. The twenty random draws of Fig. 3 reclassified across a grid of the two gate thresholds. Each cell gives the number of sparse draws (of sixteen at 12 and 24 stations) labeled collapse, and, in parentheses, the median transition-zone shift of the admitted sparse draws. The collapse fraction stays between 50 and 75% across the grid, so the gate classification is not an artifact of the chosen thresholds. The admitted-shift medians of this twenty-draw ensemble are small-sample values, superseded by Table S2.

anchor cut	misfit [0.5, 2]	misfit [0.3, 3]	misfit [0.2, 5]
20%	12/16 (+0.00)	10/16 (+0.19)	10/16 (+0.19)
25%	11/16 (+0.06)	9/16 (+0.32)	9/16 (+0.32)
30%	11/16 (+0.06)	9/16 (+0.32)	8/16 (+0.19)

The production gate is anchor 25% with misfit [0.3, 3], the central cell.

Table S2. Sampling stability of the sparse regimes. The eight-draw discovery envelope enlarged by two independent ensembles (seeds distinct from the envelope and from each other; thirty and sixty draws per sparse size). The collapse fraction is stable. The admitted shift is sign-unstable: pooled over 98 draws per size, the admitted sign splits 19 positive to 21 negative at twelve stations and 24 to 38 at twenty-four, with medians near zero. The uniformly positive admitted draws of the discovery envelope at twelve stations (3 of 3) were a small-sample fluctuation. In the sixty-draw ensemble every cumulative statistic is flat from ten draws onward, so the ensembles are converged, not merely enlarged.

ensemble	size	draws	collapse	admitted +/−	admitted median
discovery	12	8	62%	3 / 0	+0.38
discovery	24	8	50%	2 / 2	+0.14
enlargement 1	12	30	60%	5 / 7	−0.01
enlargement 1	24	30	47%	8 / 8	−0.01
enlargement 2	12	60	58%	11 / 14	−0.03
enlargement 2	24	60	30%	14 / 28	−0.05
pooled	12	98	60%	19 / 21	near 0
pooled	24	98	37%	24 / 38	near 0

The tables regenerate from the deposited `gds_b_sm_robust.py` and `gds_b_converge.py` against the locked archive.

Declarations

Data and code availability. All input data are public (INTERMAGNET, World Data Centre for Geomagnetism Kyoto, SILSO, CHAOS-7). The audit code, locked intermediate archives, the acceptance-gate ledger, and the figure generators are deposited at Zenodo (https://doi.org/10.5281/zenodo.21184326; version 1.1 adds the audit layer of this paper as a new version of the same record).

Declaration of generative AI in scientific writing. AI-assisted tools (Claude, Anthropic) were used for log summarization, bibliographic metadata checks, and language editing. The author verified all data processing, numerical results, references, figures, and interpretations, and takes full responsibility for the work.

Competing interests. The author declares no competing interests.

Funding. This research was supported by the Basic Science Research Program through the National Research Foundation of Korea (RS-2019-NR040076) funded by the Ministry of Education (2026). This work was supported by the Institute for Korea Spent Nuclear Fuel (iKSNF) and Korea Foundation of Nuclear Safety (KoFONS) grant funded by the Korea government (Nuclear Safety and Security Commission, NSSC) (RS-2021-KN066110). This work was supported by the National Research Foundation of Korea (NRF) grant funded by the Korea government (Ministry of Science and ICT, MSIT) (No. 2022R1A2C1092301).

References

- Banks, R.J., 1969. Geomagnetic variations and the electrical conductivity of the upper mantle. Geophys. J. R. Astron. Soc. 17, 457–487. https://doi.org/10.1111/j.1365-246X.1969.tb00252.x
- Civet, F., Thébault, E., Verhoeven, O., Langlais, B., Saturnino, D., 2015. Electrical conductivity of the Earth's mantle from the first Swarm magnetic field measurements. Geophys. Res. Lett. 42, 3338–3346. https://doi.org/10.1002/2015GL063397
- Daglis, I.A., Thorne, R.M., Baumjohann, W., Orsini, S., 1999. The terrestrial ring current: Origin, formation, and decay. Rev. Geophys. 37, 407–438. https://doi.org/10.1029/1999RG900009
- Dai, L., Karato, S., 2009a. Electrical conductivity of wadsleyite at high temperatures and high pressures. Earth Planet. Sci. Lett. 287, 277–283. https://doi.org/10.1016/j.epsl.2009.08.012
- Dai, L., Karato, S., 2009b. Electrical conductivity of pyrope-rich garnet at high temperature and high pressure. Phys. Earth Planet. Inter. 176, 83–88. https://doi.org/10.1016/j.pepi.2009.04.002
- Grayver, A.V., Munch, F.D., Kuvshinov, A.V., Khan, A., Sabaka, T.J., Tøffner-Clausen, L., 2017. Joint inversion of satellite-detected tidal and magnetospheric signals constrains electrical conductivity and water content of the upper mantle and transition zone. Geophys. Res. Lett. 44, 6074–6081. https://doi.org/10.1002/2017GL073446
- Huang, X., Xu, Y., Karato, S., 2005. Water content in the transition zone from electrical conductivity of wadsleyite and ringwoodite. Nature 434, 746–749. https://doi.org/10.1038/nature03426
- Karato, S., 1990. The role of hydrogen in the electrical conductivity of the upper mantle. Nature 347, 272–273. https://doi.org/10.1038/347272a0
- Karato, S., Dai, L., 2009. Comments on "Electrical conductivity of wadsleyite as a function of temperature and water content" by Manthilake et al. Phys. Earth Planet. Inter. 174, 19–21. https://doi.org/10.1016/j.pepi.2009.01.011
- Kelbert, A., Schultz, A., Egbert, G., 2009. Global electromagnetic induction constraints on transition-zone water content variations. Nature 460, 1003–1006. https://doi.org/10.1038/nature08257
- Khan, A., Kuvshinov, A., Semenov, A., 2011. On the heterogeneous electrical conductivity structure of the Earth's mantle with implications for transition zone water content. J. Geophys. Res. 116, B01103. https://doi.org/10.1029/2010JB007458
- Kuvshinov, A., Olsen, N., 2006. A global model of mantle conductivity derived from 5

years of CHAMP, Ørsted, and SAC-C magnetic data. Geophys. Res. Lett. 33, L18301. https://doi.org/10.1029/2006GL027083

- Malin, S.R.C., Winch, D.E., 1996. Annual variation of the geomagnetic field. Geophys. J. Int. 124, 170–174. https://doi.org/10.1111/j.1365-246X.1996.tb06361.x
- Min, J., Grayver, A., 2023. Simultaneous inversion for source field and mantle electrical conductivity using the variable projection approach. Earth Planets Space 75, 83. https://doi.org/10.1186/s40623-023-01816-5
- Munch, F.D., Grayver, A.V., Kuvshinov, A., Khan, A., 2018. Stochastic inversion of geomagnetic observatory data including rigorous treatment of the ocean induction effect with implications for transition zone water content and thermal structure. J. Geophys. Res. Solid Earth 123, 31–51. https://doi.org/10.1002/2017JB014691
- Oh, S., 2026a. A hidden component of magnetic storms makes Earth's mantle transition zone look drier than it is. EarthArXiv [Preprint]. https://doi.org/10.31223/X5D78K. Submitted to Science.
- Oh, S., 2026b. Gap-native time-domain geomagnetic depth sounding of mantle conductivity from hourly observatory records. Earth, Planets and Space, under review (EPSP-D-26-00179).
- Olsen, N., 1998. The electrical conductivity of the mantle beneath Europe derived from C-responses from 3 to 720 hr. Geophys. J. Int. 133, 298–308. https://doi.org/10.1046/j.1365-246X.1998.00503.x
- Olsen, N., 1999. Long-period (30 days–1 year) electromagnetic sounding and the electrical conductivity of the lower mantle beneath Europe. Geophys. J. Int. 138, 179–187. https://doi.org/10.1046/j.1365-246X.1999.00854.x
- Parker, R.L., 1980. The inverse problem of electromagnetic induction: existence and construction of solutions based on incomplete data. J. Geophys. Res. 85, 4421–4428. https://doi.org/10.1029/JB085iB08p04421
- Püthe, C., Kuvshinov, A., Olsen, N., 2015a. Handling complex source structures in global EM induction studies: from C-responses to new arrays of transfer functions. Geophys. J. Int. 201, 318–328. https://doi.org/10.1093/gji/ggv021
- Püthe, C., Kuvshinov, A., Khan, A., Olsen, N., 2015b. A new model of Earth's radial conductivity structure derived from over 10 yr of satellite and observatory magnetic data. Geophys. J. Int. 203, 1864–1872. https://doi.org/10.1093/gji/ggv407
- Semenov, A.V., Kuvshinov, A., 2012. Global 3-D imaging of mantle conductivity based on inversion of observatory C-responses — II. Data analysis and results. Geophys. J. Int. 191, 965–992. https://doi.org/10.1111/j.1365-246X.2012.05665.x
- Tarits, P., Mandéa, M., 2010. The heterogeneous electrical conductivity structure of the lower mantle. Phys. Earth Planet. Inter. 183, 115–125. https://doi.org/10.1016/j.pepi.2010.08.002
- Utada, H., Koyama, T., Shimizu, H., Chave, A.D., 2003. A semi-global reference model for electrical conductivity in the mid-mantle beneath the north Pacific region. Geophys. Res. Lett. 30, 1194. https://doi.org/10.1029/2002GL016092
- Yoshino, T., Manthilake, G., Matsuzaki, T., Katsura, T., 2008. Dry mantle transition zone inferred from the conductivity of wadsleyite and ringwoodite. Nature 451, 326–329. https://doi.org/10.1038/nature06427
- Yoshino, T., Katsura, T., 2012. Re-evaluation of electrical conductivity of anhydrous and hydrous wadsleyite. Earth Planet. Sci. Lett. 337–338, 56–67. https://doi.org/10.1016/j.epsl.2012.05.023
- Yoshino, T., Katsura, T., 2013. Electrical conductivity of mantle minerals: role of water in conductivity anomalies. Annu. Rev. Earth Planet. Sci. 41, 605–628. https://doi.org/10.1146/annurev-earth-050212-124022
- Zhang, H., Egbert, G.D., Huang, Q., 2022. A relatively dry mantle transition zone revealed by geomagnetic diurnal variations. Sci. Adv. 8, eabo3293. https://doi.org/10.1126/sciadv.abo3293